Phonon Polaritons in Monolayers of Hexagonal Boron Nitride

Siyuan Dai,* Wenjing Fang, Nicholas Rivera, Yijing Stehle, Bor-Yuan Jiang, Jialiang Shen, Roland Yingjie Tay, Christopher J. Ciccarino, Qiong Ma, Daniel Rodan-Legrain, Pablo Jarillo-Herrero, Edwin Hang Tong Teo, Michael M. Fogler, Prineha Narang, Jing Kong, and Dimitri N. Basov*

Phonon polaritons in van der Waals materials reveal significant confinement accompanied with long propagation length: important virtues for tasks pertaining to the control of light and energy flow at the nanoscale. While previous studies of phonon polaritons have relied on relatively thick samples, here reported is the first observation of surface phonon polaritons in single atomic layers and bilayers of hexagonal boron nitride (hBN). Using antenna-based near-field microscopy, propagating surface phonon polaritons in mono- and bilayer hBN microcrystals are imaged. Phonon polaritons in monolayer hBN are confined in a volume about one million times smaller than the free-space photons. Both the polariton dispersion and their wavelength–thickness scaling law are altered compared to those of hBN bulk counterparts. These changes are attributed to phonon hardening in monolayer-thick crystals. The data reported here have bearing on applications of polaritons in metasurfaces and ultrathin optical elements.

Phonon polaritons are collective modes formed by hybridization of free-space photons with lattice vibrations in polar insulators. These modes exhibit a high density of states, a strong confinement of the electric field,[1,2] and a relatively low loss comparable to that of state-of-the-art plasmonic structures.[3,4] These virtues make the polaritons promising candidates for superlensing,[5] super-Planckian heat transfer,[6] wavefront control,[7,8] and other novel applications. Besides hexagonal boron nitride (hBN),[9–15] phonon polaritons have been investigated in SiC,[5,16] GaAs,[17,18] LiTaO₃,[19] MoO₃,[20,21] as well as in metamaterials.[8,22] In these systems, phonon polaritons span a broad range of frequencies, from terahertz to mid-infrared (mid-IR).

An intriguing aspect of hBN in the context of phonon polariton physics and applications is its optical hyperbolicity,[9,10,23] i.e., the existence of a frequency band between transverse optical (TO) mode at ω_{TO} and longitudinal optical (LO) mode at ω_{LO}: $\omega_{TO} < \omega < \omega_{LO}$. In this latter frequency region, the basal-plane permittivity of hBN Re $\varepsilon^t < 0$ whereas the z-axis permittivity is positive Re $\varepsilon^z > 0$. Theory predicts[14] that the polariton dispersion within the hyperbolic frequency region consists of multiple branches whose number is equal to the number N of atomic layers. In experiment, only the so-called principal branch is typically observed, as is the case here. The theory further predicts that the

Prof. S. Dai, J. Shen
Materials Research and Education Center
Department of Mechanical Engineering
Auburn University
Auburn, AL 36849, USA
E-mail: sdai@auburn.edu

Dr. W. Fang, Prof. J. Kong
Department of Electrical Engineering & Computer Sciences
Massachusetts Institute of Technology
Cambridge, MA 02139, USA

N. Rivera, C. J. Ciccarino, Prof. P. Narang
John A. Paulson School of Engineering and Applied Sciences
Harvard University
Cambridge, MA 02139, USA

N. Rivera, Dr. Q. Ma, D. Rodan-Legrain, Prof. P. Jarillo-Herrero
Department of Physics
Massachusetts Institute of Technology
Cambridge, MA 02139, USA

Prof. Y. Stehle
Sichuan University Pittsburgh Institute
Sichuan University
Sichuan, Chengdu 610017, China

Dr. B.-Y. Jiang, Prof. M. M. Fogler
Department of Physics
University of California, San Diego
La Jolla, CA 92093, USA

R. Y. Tay, Prof. E. H. T. Teo
School of Electrical and Electronic Engineering
Nanyang Technology University
50 Nanyang Avenue, Singapore 639798, Singapore

Prof. D. N. Basov
Department of Physics
Columbia University
New York, NY 10027, USA
E-mail: db3056@columbia.edu

ADVANCED
SCIENCE NEWS
www.advancedsciencenews.com

ADVANCED
MATERIALS
www.advmat.de

dispersion of this branch near the in-plane TO frequency ω_{TO} = 1367 cm^{-1} is linear in polariton momentum k

$$\omega = \omega_{TO} + N\nu_1 k, \quad k_0 << k << 1/(Nd_1) \qquad (1)$$

Here, k_0 is the momentum of the IR photon, $\lambda_0 = 2\pi/k_0$ is the corresponding wavelength, d_1 = 0.34 nm is the hBN interlayer distance, and ν_1 is a characteristic velocity discussed below. Equation (1) implies that the polariton dispersion can be tuned by varying N, which has been verified by imaging of phonon polariton propagation in real space.[9] (Tuning of the polariton dispersion by electrostatic gating[22] and temperature[24,25] has also been demonstrated.) Because of weak van der Waals (vdW) coupling of the layers, N can be controlled with atomic precision using exfoliation or chemical-vapor-deposition techniques. However, imaging of phonon polaritons has so far been achieved only in multilayer (bulk) hBN crystals.[8,9] In the present work, we report imaging of phonon polaritons in monolayer and bilayer hBN. Our principal finding is that polariton modes harden (shift to higher frequency) in hBN monolayers: the ultimate limit of a single atomic plane. A possible reason for the phonon hardening may be a small decrease of the in-plane lattice constant compared to the bulk value due to the lack of interlayer interaction.[26,27] Theoretical calculations of this effect have not yet reached a consensus, predicting either softening[15] or hardening[26] of the phonon mode. Therefore, our experimental results provide an empirical reference point for the lattice dynamics models of atomically thin vdW layers. Our results may also be relevant for the development of ultrathin phononic elements for mid-IR optics.[28] Note that in monolayers, the notion of the z-axis permittivity and therefore hyperbolic collective modes[10,11,13,14] is not applicable. The phonon polaritons we have imaged are better understood as surface modes. Their field distribution decays exponentially away from hBN. Nevertheless, Equation (1) remains valid even for $N = 1$ as we will discuss below and also in the Supporting Information (Sections S2 and S3).

Our monolayer and bilayer hBN samples were grown[29] by low-pressure chemical vapor deposition (LP-CVD) method on iron foils and then transferred to the SiO$_2$/Si substrates (see the Experimental Section for details). We performed the IR nanoimaging of these samples using the scattering-type scanning near-field optical microscopy (s-SNOM).[16] The s-SNOM, based on a tapping-mode atomic force microscope (AFM), simultaneously yields the topography and nano-IR images over the scanned area. In the experiment, a continuous-wave IR laser (solid arrow) is focused on the apex of a metalized AFM tip, which acts as an optical antenna generating a strong near field (**Figure 1**a). This field launches phonon polaritons in hBN[30] that propagate to the edge of the sample and get reflected back to the tip. The modified near field under the tip creates scattered IR light, which is detected in the far field. The experimental observables are the near-field amplitude $S(\omega)$ and phase $\Phi(\omega)$ detected in the back-scattering geometry and demodulated at the third harmonics of the tip tapping frequency. The demodulation eliminates far-field background and isolates the genuine near-field signal.[31]

Our representative s-SNOM images are shown in Figure 1b–d. The hBN crystals have triangular shapes[32] and exhibit an evident s-SNOM phase $\Phi(\omega)$ contrast that can be clearly distinguished from that of the SiO$_2$ substrate. Close to sample edges, we find oscillations or fringes characteristic of polaritonic standing waves in 2D materials.[1,2] These fringes are aligned parallel to the hBN edges in both monolayer and bilayer crystals. Line traces (taken along the blue and red dotted lines in Figure 1b) demonstrate polariton fringes as peaks and valleys in **Figure 2**a,b. The fringes are observed only at frequencies above the in-plane TO frequency of bulk hBN, ω_{TO} = 1367 cm^{-1}. Our imaging data reveal a systematic evolution of the fringes with ω (Figure 1b–d): as ω increases, the fringes move closer to the hBN edge ($L = 0$, see also line profiles in Figure 2a,b), indicating a decreasing period of the fringes. Such hallmarks of dispersive phenomena validate the assignment of the fringes to surface phonon polaritons[33] in hBN. The fringes form along the hBN edges due to the interference of the tip-launched and edge-reflected surface phonon polaritons.[9,11,13,34] Note that the phase images are better suited for visualizing phonon polaritons in ultrathin samples (Figure 1) because the fringes in $\Phi(\omega)$ are closer to the crystal edges[11,35] compared with those in $S(\omega)$ and so suffer less damping. Nevertheless, we utilized both $\Phi(\omega)$ and $S(\omega)$ for the quantitative analysis (see Section S1 of Supporting
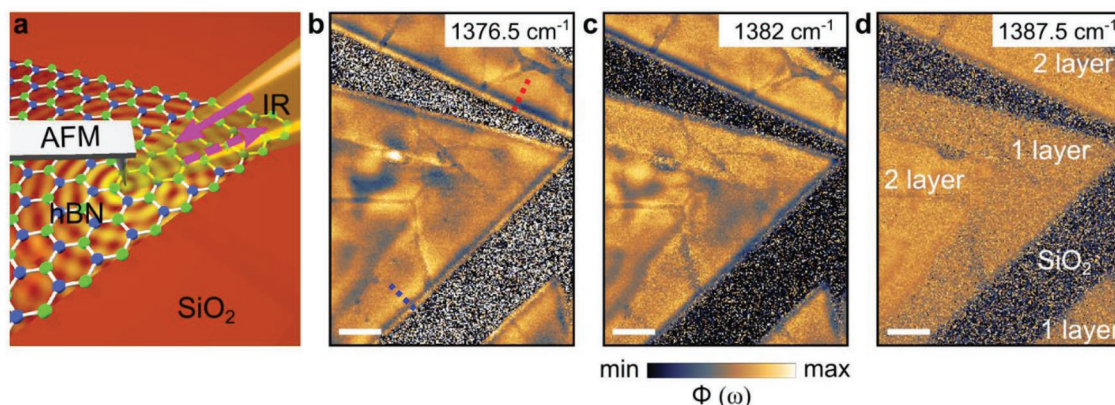

Figure 1. Nanoimaging of surface phonon polaritons in monolayer and bilayer hBN. a) Experiment setup. The AFM tip and hBN sample are illuminated by the IR beam (solid magenta arrow) from a QCL. Propagating surface phonon polariton waves are launched and detected by the AFM tip (dotted magenta arrow). b–d) s-SNOM phase images of surface phonon polaritons in monolayer and bilayer hBN at IR frequency ω = 1376.5, 1382, and 1387.5 cm^{-1}. Scale bar: 500 nm.
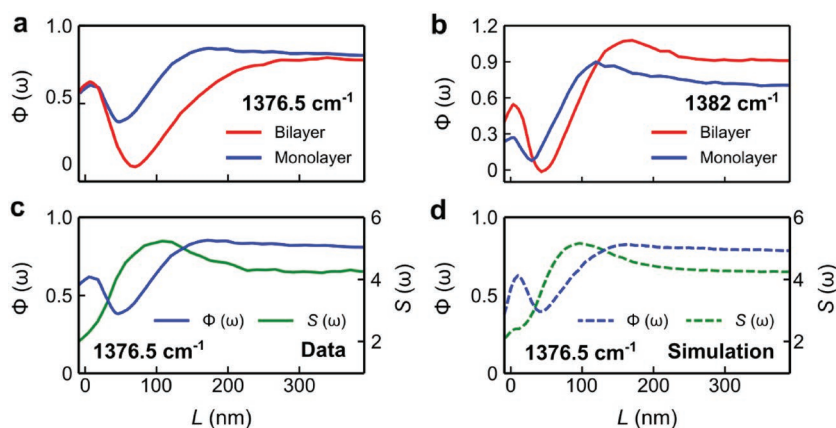
Figure 2. Line traces of the surface phonon polaritons in monolayer and bilayer hBN. Line traces of s-SNOM phase $\Phi(\omega)$ taken along the dotted cuts in Figure 1 at IR frequency a) $\omega = 1376.5$ cm^{-1} and b) 1382 cm^{-1}. c) Line traces of s-SNOM phase $\Phi(\omega)$ and amplitude $S(\omega)$ at $\omega = 1376.5$ cm^{-1}. d) Simulation of s-SNOM phase $\Phi(\omega)$ and amplitude $S(\omega)$ at $\omega = 1376.5$ cm^{-1}.

Information). For each frequency ω, we extracted the polariton wavelength λ and the dimensionless damping factor γ by fitting the s-SNOM line profiles of $\Phi(\omega)$ and $S(\omega)$ (Figure 2a,b) to numerically calculated line ones (Supporting Information, Section S1). We also extracted λ by another, simpler method, based on evaluating the peak-to-valley distance in the $\Phi(\omega)$ line traces. The two methods gave consistent results. The inferred dispersion of the phonon polaritons is displayed in **Figure 3** where we plot frequency ω versus the confinement factor $\lambda_0/\lambda = k/k_0$. Figure 3a shows the results for a bilayer (triangles) and Figure 3b for a monolayer (dots). In both cases, the confinement factor λ_0/λ can approach or exceed 60 (Figure 3). Accordingly, the mode volume $\lambda^3/\pi^{[22]}$ of polaritons is reduced compared to the mode volume $(\lambda_0)^3$ of free-space photons[36] by a factor up to 10^6.

We now compare the experimental dispersions with Equation (1). There are several complementary theoretical approaches to deriving the characteristic velocity v_1 in Equation (1) (see the Supporting Information, Section S2); among these, continuum electrodynamics is the simplest approach. This approach predicts that v_1 is determined by the in-plane permittivity ε^t of hBN and the permittivity ε_2 of SiO$_2$ substrate. The z-axis permittivity of hBN gives only subleading corrections because of the strong inequality $|\varepsilon^t| \gg \varepsilon^z$ near ω_{TO}. This explains why continuum electrodynamics is valid not only for relatively thick[9,23,34] but also for atomically thin hBN crystals. The red dash-dotted line in Figure 3a corresponding to permittivity ($\omega_{TO} = 1367$ cm^{-1}, $\omega_{LO} = 1614$ cm^{-1}, etc.)[4,10] is in a quantitative agreement with our data for bilayer hBN (triangles). On the other hand, the blue dashed line in Figure 3b corresponding to the same ω_{TO} and v_1 systematically underestimates the polariton frequency measured in a monolayer (dots). In addition, the linear thickness-dependence

law for phonon polaritons in bulk hBN[9,23,34] fails in the case of monolayer and bilayer samples. Provided ω_{TO} and v_1 were the same in the monolayer and the bilayer, the ratio of their polariton wavelengths at a given frequency would be equal to 2 (blue dashed line). Instead, the ratio is frequency-dependent and varies from 1.1 to 1.7 (**Figure 4**, black squares). We can account for both discrepancies by assuming that the TO frequency of the monolayer is blueshifted by 3.5 cm^{-1}, giving the dispersion indicated by the green dashed line in Figure 4. Previously, similar mode hardening has been observed in Raman spectroscopy of monolayer hBN[27] and BN nanotubes.[26]

As mentioned above, one possible explanation for the blueshift of phonon resonances in ultrathin hBN is a slight shortening of the B−N bonds[26] due to the lack of interlayer interaction. To further verify this hypothesis we have performed density functional theory calculations[37] taking into account exchange-correlation functionals and vdW interaction. Our calculations reveal a 2 cm^{-1} blueshift of the phonon in monolayer compared with that in bilayer hBN (Supporting Information, Section S2). We note that the phonon mode hardening due to the lack of interlayer interactions is likely to be generic to monolayers of vdW materials, including black phosphorus, transition metal dichalcogenides,[38] nanotubes,[12] and in-plane heterostructures.[39,40]

Because of the signal-to-noise limitations of state-of-the-art nano-IR methods that we utilized in our work, our imaging of surface phonon polaritons in monolayer was restricted to the vicinity of the TO phonon frequency where the dielectric loss in hBN is strong (polariton damping factor $\gamma \sim 0.6$). With an improved spatial resolution, it may become possible to image polaritons at higher frequencies where the dielectric
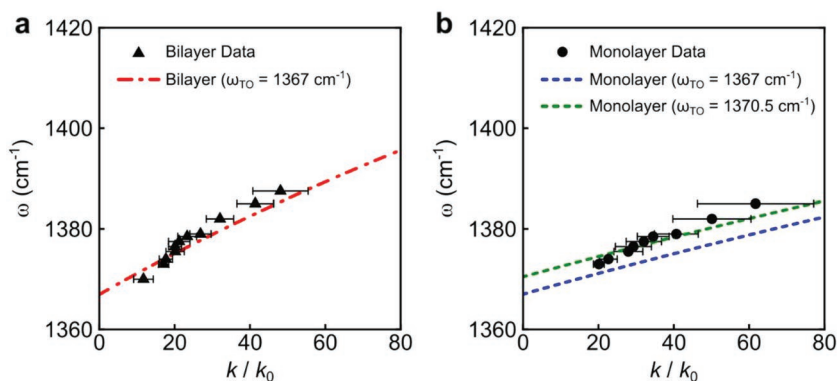

Figure 3. Dispersion of surface phonon polaritons in monolayer and bilayer hBN. a) Frequency (ω)–momentum (k/k_0) dispersion of surface phonon polaritons in bilayer hBN. b) Frequency (ω)–momentum (k/k_0) dispersion of surface phonon polaritons in monolayer hBN. Experimental data (dots for monolayer and triangles for bilayer) are extracted from s-SNOM images in Figure 1. Theoretical results are indicated with blue ($\omega_{TO} = 1367$ cm^{-1}) and green ($\omega_{TO} = 1370.5$ cm^{-1}) dashed curves for monolayer hBN and red ($\omega_{TO} = 1367$ cm^{-1}) dashed-dotted curve for bilayer hBN.

**ADVANCED
SCIENCE NEWS**

www.advancedsciencenews.com

**ADVANCED
MATERIALS**

www.advmat.de

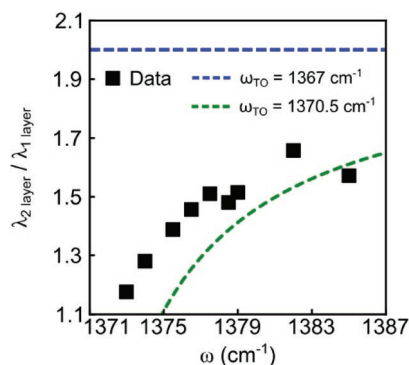**Figure 4.** The wavelength ratio between surface phonon polaritons in bilayer (λ_{2layer}) and in monolayer hBN (λ_{1layer}). Experimental data are plotted with black squares. Theoretical results are plotted with the green (monolayer hBN: $\omega_{TO} = 1370.5$ cm^{-1}) and blue (monolayer hBN: $\omega_{TO} = 1367$ cm^{-1}) dashed curve.

loss is smaller.[9] We envision a possibility of tuning phonon polaritons in thin vdW crystals with strain and friction engineering.[41–43] Finally, it may be worth exploring a 1D counterpart of hyperbolic surface polaritons propagating along the hBN edges.[44,45]

Experimental Section

Experimental Setup: The IR nanoimaging of surface phonon polaritons in monolayer and bilayer hBN were performed using an s-SNOM. This s-SNOM, based on a tapping-mode AFM, is a commercial system (www.neaspec.com). In order to launch and detect propagating polaritons, a commercial AFM tip (tip radius ≈10 nm) with a PtIr$_5$ coating was used. In the experiment, the AFM tip was illuminated by monochromatic quantum cascade lasers (QCLs) (www.daylightsolutions.com) covering a frequency range of 900–2300 cm^{-1} in the mid-IR. The phase and amplitude s-SNOM nanoimages were recorded by a pseudo-heterodyne interferometric detection module with an AFM tapping frequency 280 kHz and tapping amplitude around 70 nm. To obtain the background-free signal, the s-SNOM output at the third harmonics of the tapping frequency was demodulated.

Sample Synthesis: Monolayer and bilayer hBN were synthesized using LP-CVD with borazine as the precursor. Before the synthesis of hBN, the Fe foil (Alfa Aesar, 99.99%) was pretreated by annealing it at 1100 °C for 1 h under 10 sccm H$_2$. During the hBN growth, 0.1 sccm H$_2$ carrier gas (with borazine vapor) and 100 sccm H$_2$ at 1100 °C for 1 h were supplied. After the growth, the sample was first cooled with a rate of 5 °C min^{-1} until 700 °C and then to the room temperature without a controlled rate.

To transfer the synthesized hBN, the sample was first coated with a layer of poly(methyl methacrylate) (PMMA, 950 A9, MicroChem, diluted to 4.5% in anisole) at 2500 rpm for 1 min and baked it at 80 °C for 10 min. Before transferring the sample to the SiO2/Si substrate, Fe foil was removed by floating the coated sample on nitric acid (Transene Company Inc.) for 1 h. Finally, the PMMA was washed out by acetone and thermal annealing at 350 °C under 200 sccm H$_2$ and 200 sccm Ar for 3 h.

Supporting Information

Supporting Information is available from the Wiley Online Library or from the author.

Conflict of Interest

The authors declare no conflict of interest.

[1] D. N. Basov, M. M. Fogler, F. J. García de Abajo, *Science* **2016**, *354*, aag1992.

[2] T. Low, A. Chaves, J. D. Caldwell, A. Kumar, N. X. Fang, P. Avouris, T. F. Heinz, F. Guinea, L. Martin-Moreno, F. Koppens, *Nat. Mater.* **2016**, *16*, 182.

[3] Z. Fei, A. S. Rodin, G. O. Andreev, W. Bao, A. S. McLeod, M. Wagner, L. M. Zhang, Z. Zhao, M. Thiemens, G. Dominguez, M. M. Fogler, A. H. C. Neto, C. N. Lau, F. Keilmann, D. N. Basov, *Nature* **2012**, *487*, 82.

[4] G. X. Ni, A. S. McLeod, Z. Sun, L. Wang, L. Xiong, K. W. Post, S. S. Sunku, B. Y. Jiang, J. Hone, C. R. Dean, M. M. Fogler, D. N. Basov, *Nature* **2018**, *557*, 530.

[5] T. Taubner, D. Korobkin, Y. Urzhumov, G. Shvets, R. Hillenbrand, *Science* **2006**, *313*, 1595.

[6] S. Shen, A. Narayanaswamy, G. Chen, *Nano Lett.* **2009**, *9*, 2909.

[7] T. Feurer, N. S. Stoyanov, D. W. Ward, J. C. Vaughan, E. R. Statz, K. A. Nelson, *Annu. Rev. Mater. Res.* **2007**, *37*, 317.

[8] P. Li, I. Dolado, F. J. Alfaro-Mozaz, F. Casanova, L. E. Hueso, S. Liu, J. H. Edgar, A. Y. Nikitin, S. Vélez, R. Hillenbrand, *Science* **2018**, *359*, 892.

[9] S. Dai, Z. Fei, Q. Ma, A. S. Rodin, M. Wagner, A. S. McLeod, M. K. Liu, W. Gannett, W. Regan, K. Watanabe, T. Taniguchi,

**ADVANCED
SCIENCE NEWS**

www.advancedsciencenews.com

**ADVANCED
MATERIALS**

www.advmat.de

M. Thiemens, G. Dominguez, A. H. C. Neto, A. Zettl, F. Keilmann, P. Jarillo-Herrero, M. M. Fogler, D. N. Basov, *Science* **2014**, *343*, 1125.

[10] J. D. Caldwell, A. V. Kretinin, Y. Chen, V. Giannini, M. M. Fogler, Y. Francescato, C. T. Ellis, J. G. Tischler, C. R. Woods, A. J. Giles, M. Hong, K. Watanabe, T. Taniguchi, S. A. Maier, K. S. Novoselov, *Nat. Commun.* **2014**, *5*, 5221.

[11] Z. Shi, H. A. Bechtel, S. Berweger, Y. Sun, B. Zeng, C. Jin, H. Chang, M. C. Martin, M. B. Raschke, F. Wang, *ACS Photonics* **2015**, *2*, 790.

[12] X. G. Xu, B. G. Ghamsari, J.-H. Jiang, L. Gilburd, G. O. Andreev, C. Zhi, Y. Bando, D. Golberg, P. Berini, G. C. Walker, *Nat. Commun.* **2014**, *5*, 4782.

[13] E. Yoxall, M. Schnell, A. Y. Nikitin, O. Txoperena, A. Woessner, M. B. Lundeberg, F. Casanova, L. E. Hueso, F. H. L. Koppens, R. Hillenbrand, *Nat. Photonics* **2015**, *9*, 674.

[14] K. H. Michel, B. Verberck, *Phys. Rev. B* **2011**, *83*, 115328.

[15] T. Sohier, M. Gibertini, M. Calandra, F. Mauri, N. Marzari, *Nano Lett.* **2017**, *17*, 3758.

[16] R. Hillenbrand, T. Taubner, F. Keilmann, *Nature* **2002**, *418*, 159.

[17] M. Haraguchi, M. Fukui, S. Muto, *Phys. Rev. B* **1990**, *41*, 1254.

[18] T. Dekorsy, V. A. Yakovlev, W. Seidel, M. Helm, F. Keilmann, *Phys. Rev. Lett.* **2003**, *90*, 055508.

[19] T. Feurer, J. C. Vaughan, K. A. Nelson, *Science* **2003**, *299*, 374.

[20] W. Ma, P. Alonso-González, S. Li, A. Y. Nikitin, J. Yuan, J. Martín-Sánchez, J. Taboada-Gutiérrez, I. Amenabar, P. Li, S. Vélez, C. Tollan, Z. Dai, Y. Zhang, S. Sriram, K. Kalantar-Zadeh, S.-T. Lee, R. Hillenbrand, Q. Bao, *Nature* **2018**, *562*, 557.

[21] Z. Zheng, N. Xu, S. L. Oscurato, M. Tamagnone, F. Sun, Y. Jiang, Y. Ke, J. Chen, W. Huang, W. L. Wilson, A. Ambrosio, S. Deng, H. Chen, *Sci. Adv.* **2019**, *5*, eaav8690.

[22] S. Dai, Q. Ma, M. K. Liu, T. Andersen, Z. Fei, M. D. Goldflam, M. Wagner, K. Watanabe, T. Taniguchi, M. Thiemens, F. Keilmann, G. C. A. M. Janssen, S. E. Zhu, P. Jarillo-Herrero, M. M. Fogler, D. N. Basov, *Nat. Nanotechnol.* **2015**, *10*, 682.

[23] S. Dai, Q. Ma, T. Andersen, A. S. McLeod, Z. Fei, M. K. Liu, M. Wagner, K. Watanabe, T. Taniguchi, M. Thiemens, F. Keilmann, P. Jarillo-Herrero, M. M. Fogler, D. N. Basov, *Nat. Commun.* **2015**, *6*, 6963.

[24] T. G. Folland, A. Fali, S. T. White, J. R. Matson, S. Liu, N. A. Aghamiri, J. H. Edgar, R. F. Haglund, Y. Abate, J. D. Caldwell, *Nat. Commun.* **2018**, *9*, 4371.

[25] S. Dai, J. Zhang, Q. Ma, S. Kittiwatanakul, A. McLeod, X. Chen, S. G. Corder, K. Watanabe, T. Taniguchi, J. Lu, Q. Dai, P. Jarillo-Herrero, M. Liu, D. N. Basov, *Adv. Mater.* **2019**, *31*, 1900251.

[26] R. Arenal, A. C. Ferrari, S. Reich, L. Wirtz, J. Y. Mevellec, S. Lefrant, A. Rubio, A. Loiseau, *Nano Lett.* **2006**, *6*, 1812.

[27] R. V. Gorbachev, I. Riaz, R. R. Nair, R. Jalil, L. Britnell, B. D. Belle, E. W. Hill, K. S. Novoselov, K. Watanabe, T. Taniguchi, A. K. Geim, P. Blake, *Small* **2011**, *7*, 465.

[28] H.-T. Chen, A. J. Taylor, N. Yu, *Rep. Prog. Phys.* **2016**, *79*, 076401.

[29] S. M. Kim, A. Hsu, M. H. Park, S. H. Chae, S. J. Yun, J. S. Lee, D.-H. Cho, W. Fang, C. Lee, T. Palacios, M. Dresselhaus, K. K. Kim, Y. H. Lee, J. Kong, *Nat. Commun.* **2015**, *6*, 8662.

[30] S. Dai, Q. Ma, Y. Yang, J. Rosenfeld, M. D. Goldflam, A. McLeod, Z. Sun, T. I. Andersen, Z. Fei, M. Liu, Y. Shao, K. Watanabe, T. Taniguchi, M. Thiemens, F. Keilmann, P. Jarillo-Herrero, M. M. Fogler, D. N. Basov, *Nano Lett.* **2017**, *17*, 5285.

[31] N. Ocelic, A. Huber, R. Hillenbrand, *Appl. Phys. Lett.* **2006**, *89*, 101124.

[32] K. K. Kim, A. Hsu, X. Jia, S. M. Kim, Y. Shi, M. Hofmann, D. Nezich, J. F. Rodriguez-Nieva, M. Dresselhaus, T. Palacios, J. Kong, *Nano Lett.* **2012**, *12*, 161.

[33] D. C. Joshua, L. Lindsay, V. Giannini, I. Vurgaftman, L. R. Thomas, A. M. Stefan, J. G. Orest, *Nanophotonics* **2015**, *4*, 44.

[34] A. J. Giles, S. Dai, I. Vurgaftman, T. Hoffman, S. Liu, L. Lindsay, C. T. Ellis, N. Assefa, I. Chatzakis, T. L. Reinecke, J. G. Tischler, M. M. Fogler, J. H. Edgar, D. N. Basov, J. D. Caldwell, *Nat. Mater.* **2017**, *17*, 134.

[35] J. A. Gerber, S. Berweger, B. T. O'Callahan, M. B. Raschke, *Phys. Rev. Lett.* **2014**, *113*, 055502.

[36] D. Alcaraz Iranzo, S. Nanot, E. J. C. Dias, I. Epstein, C. Peng, D. K. Efetov, M. B. Lundeberg, R. Parret, J. Osmond, J.-Y. Hong, J. Kong, D. R. Englund, N. M. R. Peres, F. H. L. Koppens, *Science* **2018**, *360*, 291.

[37] N. Rivera, T. Christensen, P. Narang, *Nano Lett.* **2019**, *19*, 2653.

[38] A. Nemilentsau, T. Low, G. Hanson, *Phys. Rev. Lett.* **2016**, *116*, 066804.

[39] Z. Liu, L. Ma, G. Shi, W. Zhou, Y. Gong, S. Lei, X. Yang, J. Zhang, J. Yu, K. P. Hackenberg, A. Babakhani, J.-C. Idrobo, R. Vajtai, J. Lou, P. M. Ajayan, *Nat. Nanotechnol.* **2013**, *8*, 119.

[40] L. Liu, J. Park, D. A. Siegel, K. F. McCarty, K. W. Clark, W. Deng, L. Basile, J. C. Idrobo, A.-P. Li, G. Gu, *Science* **2014**, *343*, 163.

[41] S. R. Sales de Mello, M. E. H. Maia da Costa, C. M. Menezes, C. D. Boeira, F. L. Freire, F. Alvarez, C. A. Figueroa, *Sci. Rep.* **2017**, *7*, 3242.

[42] S. Kajita, M. Tohyama, H. Washizu, T. Ohmori, H. Watanabe, S. Shikata, *Tribol. Online* **2015**, *10*, 156.

[43] B. Lyu, H. Li, L. Jiang, W. Shan, C. Hu, A. Deng, Z. Ying, L. Wang, Y. Zhang, H. A. Bechtel, M. C. Martin, T. Taniguchi, K. Watanabe, W. Luo, F. Wang, Z. Shi, *Nano Lett.* **2019**, *19*, 1982.

[44] S. Dai, M. Tymchenko, Y. Yang, Q. Ma, M. Pita-Vidal, K. Watanabe, T. Taniguchi, P. Jarillo-Herrero, M. M. Fogler, A. Alù, D. N. Basov, *Adv. Mater.* **2018**, *30*, 1706358.

[45] P. Li, I. Dolado, F. J. Alfaro-Mozaz, A. Y. Nikitin, F. Casanova, L. E. Hueso, S. Vélez, R. Hillenbrand, *Nano Lett.* **2017**, *17*, 228.